Materials Advances

ROYAL SOCIETY OF CHEMISTRY

PAPER

View Article Online
View Journal | View Issue

Cite this: *Mater. Adv.*, 2024, 5, 9781

Thermoelectric signature of d-orbitals in tripod-based molecular junctions†

Oday A. Al-Owaedi,*[ab] Hussein Neama Najeeb,[a] Ahmed Kareem Obaid Aldulaimi,[bc] Nathera Hussin Alwan,[b] Mohammed Shnain Ali,[bd] Majed H. Dwech[be] and Muneer A. AL-Da'amy[f]

Received 25th June 2024,
Accepted 8th November 2024

DOI: 10.1039/d4ma00646a

rsc.li/materials-advances

Promoting the thermoelectric properties of single-molecule junctions is a significant goal of a wide range of studies. Herein, the excellent consistency between current theoretical results and the experimental outcomes of previous studies helped establish a robust strategy for incorporating different transition metals into tripod connectors. This strategy proves that the involved dπ–pπ conjugation can not only enhance the electrical conductance, similar to that of conjugated hydrocarbons, but also improve the thermoelectric properties through interactions induced by the metal centre. The incorporation of the metal leads to an unconventional stereoelectronic effect caused by the metal–carbon dπ–pπ hyperconjugation. The odd number of electrons in the d-orbitals of molecular junctions with transition-metal centres presents a clear signature in the enhanced Seebeck coefficient, making them promising candidates for thermoelectric applications.

Introduction

Single-molecule technology is currently considered a technology of the future due to the small size and diversity of molecules, which may lead to the construction of functional devices with unique properties. However, it currently faces challenges related to the small size and diversity of molecules.[1,2] In the field of molecular electronics, the design of one-dimensional molecular wires with a single type of anchor group has captured much of the research interest to date.[3,4] This motif is simple and could present interesting structure–property relationships and conductance mechanisms without excessive complication.[5] However, the difficulty associated with these structures lies in the spatial limitations of the single molecule, which is usually unstable, making junction formation challenging. Therefore, the use of a tripodal structure has been proposed by several groups.[6–18] In this context, the number and type of anchor groups are crucial in creating stable junctions.[19] M. A. Karimi[20] and others[21] have reported that the probability of molecular-junction formation increases significantly in the presence of tripod connectors, as these connectors can enhance the stability of the molecular junction. Yutaka Ie *et al.*[22] innovatively prepared a single-molecule junction involving a pyridine-based tripodal anchor unit. The conductance of this structure was $5 \pm 1 \times 10^{-4}$ G_0, which is considered high compared to other junctions with different anchor groups.[23,24] Future thermoelectric and electronic applications of single molecules may not only require high and low conductance, but also a range of modulations to adjust the precise characteristics of the circuit.[25,26] The broad palette of ions available in organometallic molecules makes them appropriate candidates for producing a wide range of electrical conductance and thermoelectric capabilities.[27–31] At the same time, transition metals exhibit various electronic effects that already play an important role in single-molecule devices,[32,33] molecular thermoelectrics,[34,35] and molecular spintronic devices,[36,37] which rely on redox interactions.[38,39] In addition, metals have diverse bonding patterns with light elements through participation of the metal's d-subshell, resulting in secondary interactions.[40] For instance, the hyperconjugation impact[41,42] could be mediated by the metal centre, leading to dramatic modifications in the reaction mechanism.[43,44] Furthermore, the understanding of the secondary interactions could be a useful way to interpret the interactions between the metal and light elements,[45,46] which is important in organometallic catalysis.[47,48] Although, the influence of secondary interactions is important and can significantly enhance the performance of molecular electronic devices, it has been largely disregarded to

[a] *Department of Laser Physics, College of Science for Women, University of Babylon, Hilla 51001, Iraq. E-mail: oday.alowaedi@uobabylon.edu.iq*
[b] *Al-Zahrawi University College, KarbalaNajaf-Karbala Street, 56001, Iraq*
[c] *College of Food Science, Al-Qasim Green University, Babylon, Al-Qasim, 51001, Iraq*
[d] *College of Medicine, University of Karbala, Karbala, 56001, Iraq*
[e] *College of Science, University of Karbala, Karbala, 56001, Iraq*
[f] *College of Education for Pure Science, University of Karbala, Karbala, 56001, Iraq*

† Electronic supplementary information (ESI) available: Involves theories and all details relevant to the computational methods. The author have cited additional references (ref. 108–111). See DOI: 10.1039/d4ma00646a

date. In this context, the current investigation adopted a new strategy by incorporating d-orbital metals with tripod connectors to explore the electronic and thermoelectric properties of tripod-based molecular junctions.

Results and discussion

A tripodal-molecular platform pictures a perpendicular contact to the electrode, which represents a powerful way to establish a conducting path between two electrodes.[49–53] Fig. 1(a) shows six of these platforms chosen for study here. They involve with different metals (Mg, Co, Ni, Cu, Zn, and Pt) as a metal centre. The metal is connected to three phenyl rings *via* three single bonds, and a double bond to the sulfur atom. Each molecule is categorized as a three-dimensional compound consisting of three identical molecular wires linked to methyl sulfide (SMe) anchor groups. The first molecule (M-1) contains magnesium (Mg) atom as a metal centre. Like the other alkaline earth metals, it has a filled *s* orbital and two valence electrons. Unlike the transition metals, it does not have any partially filled d-orbitals in its atomic structure,[54] and it was chosen here for comparison with the transition metals. Cobalt (Co) is the metal centre of molecule M-2, as shown in Fig. 1(a). Cobalt is one of the transition metals and is in the 7th column of the d-block and therefore has 7d electrons. Molecule M-3 possesses the nickel (Ni) atom as a metal centre, with 8 electrons in its d-orbital. Copper (Cu) and zinc (Zn) atoms are the metal centres of molecules M-4 and M-5, respectively, which are classified as transition metals with 10 electrons in their d-orbitals. The d-orbital of the platinum (Pt) atom is partially occupied by 9 electrons for molecule M-6.

Fig. 1(b) depicts the orientations of the d-orbitals for all these molecules with transition-metal centres. The first one (M-2) is d_{z^2}, which possesses the shape of a single dumbbell along the *Z*-axis, with a doughnut-like ring around the nucleus on the *x*–*y* plane, while the second one (M-3) is $d_{x^2-y^2}$ and is similar to the shape of a clover leaf, but its leaves are oriented along the *X* and *Y* axes. The d-orbitals of molecules M-2 and M-6 are characterized by doughnut-like shapes, whereas the d-orbitals of the M-3, M-4, and M-5 molecules are distinguished by a clover-leaf shape. It is worth mentioning that odd numbers of electrons (7 and 9 electrons) belong to the d-orbitals of the M-2 and M-6 molecules, respectively. In contrast, the d-orbitals of molecules M-3, M-4, and M-5 have an even number of electrons (8, 10, and 10 electrons, respectively). In addition, Fig. 1(b) shows that the lowest energies of the LUMO orbitals (0.38 and 0.6 eV) were presented by M-6 and M-2, respectively, while the highest energies (1.12, 0.88, and 0.74 eV) were exhibited by M-5, M-4, and M-3, respectively. These results could be explicated in terms of the crystal field theory (CFT), a bonding model that elucidates many important characteristics of transition-metal complexes, including their structures, stability, and reactivity.[55] If the negative charges are distributed uniformly over the surface of a sphere, the d-orbitals of Zn-metal, for example, will remain degenerate, but their energy will be higher due to the repulsive electrostatic interactions between the spherical shell with the negative charge and the electrons in the d-orbitals. The placing of negative charges

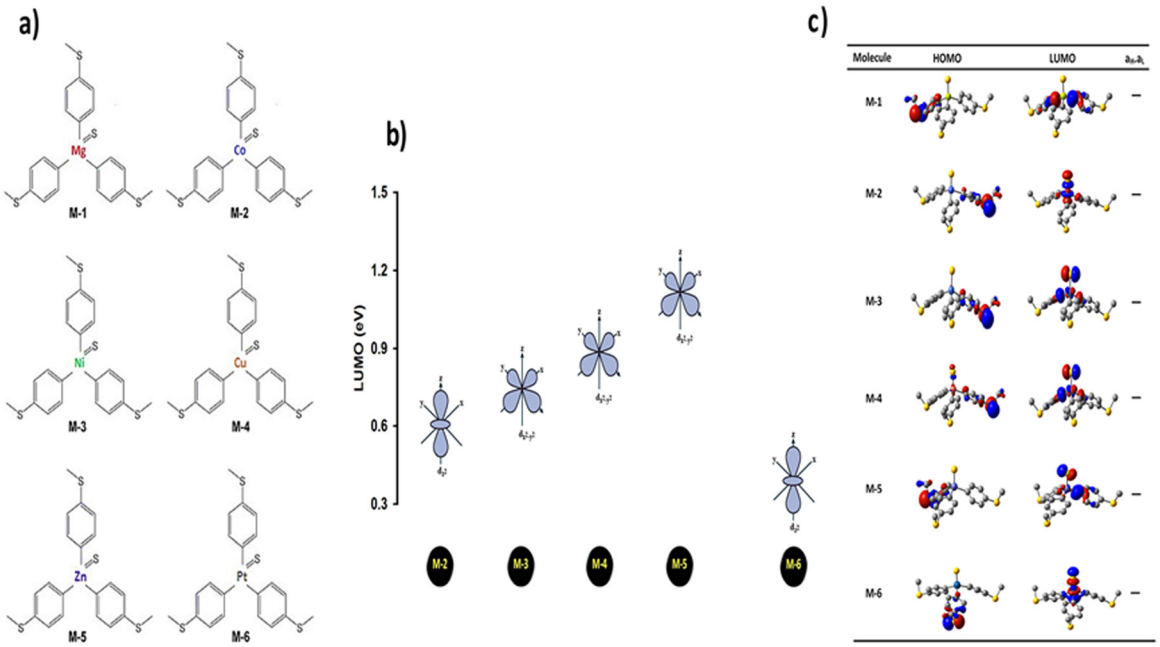

Fig. 1 (a) Schematic illustration of tripod connectors with six different metal centres; (b) schematic showing the d-orbital shape of some transition metals (Co, Ni, Cu, Zn, and Pt respectively); (c) optimized geometry of all the molecules in a gas phase, and their HOMOs and LUMOs (isosurfaces ±0.02 (e bohr^{-3})$^{1/2}$). The blue part is a positive sign, while the red part is a negative sign. $a_H \cdot a_L$ is the multiplication of the HOMO and LUMO amplitudes. As an example, the HOMO and LUMO for the M-1 molecule possess different signs, and thus the multiplication of the molecular orbitals amplitudes ($a_H \cdot a_L$) is a negative sign and the molecule exhibits constructive quantum interference (CQI).

at the vertices of an octahedron does not change the average energy of the d-orbitals, but it does remove their degeneracy. The five d-orbitals split into two groups ($d_{x^2-y^2}$ and d_{z^2}), whose energies depend on their orientations, as shown in Fig. 1(b). To obtain a better understanding of the transport behaviour, the electronic properties of all the molecules in a gas phase were investigated using the DFT method (at the B3LYP level of theory[56] with a LANL2DZ basis set[57,58]), as shown in Fig. 1(c). The LUMOs of all complexes, except M-1, displayed a pattern of dπ–pπ interactions along the metal–phenyl axis[59] with a large metal character, while the HOMOs exhibited a small metal character. Fig. 1 suggests that the positively charged metal centres (LUMOs) for Co, Ni, Cu, Zn, and Pt atoms can be viewed as excellent electron acceptors, reflecting an interact with the occupied pπ orbital of the carbon atoms. The crystal field theory (CFT) proposes that the positively charged metal centre of molecules could generate an unexpected metal–carbon interaction. These results could be ascribed to the generation of a positively charged metal centre because the protonation occupied a place on the metal carbyne unit of the molecule.

Mülliken population analysis[60] of the frontier orbitals of all the molecules indicated that the orbitals make a huge contribution to the LUMO but only a little one to the HOMO, which could be an indication of a LUMO-dominated transport mechanism,[25,60–62] which is consistent with the transport behaviour shown in Fig. 2. Herein, orbital analysis was performed to provide further insights into the transport characteristics of the junctions. Lambert *et al.*[63] reported an orbital symmetry rule. The magic ratio theory[64] is based on utilizing the exact core Green's function, defined by:

$$g(E) = (\mathrm{IE} - \mathrm{H})^{-1} \quad (1)$$

In the literature, various approximations for $g(E)$ are discussed, one of which involves the approximation including only the contributions to the $g(E)$ from the HOMO and LUMO. If the amplitudes of the HOMO on sites a and b are denoted as $\psi_a^{E_H}$ and $\psi_b^{E_H}$ and the amplitudes of the LUMO are $\psi_a^{E_L}$ and $\psi_b^{E_L}$, then if the contributions from all other orbitals are ignored, a crude approximation to the Green's function $g_{ba}(E)$ can be given by

$$g_{ab}(E) \approx \frac{\psi_a^{(E_H)}\psi_b^{(E_H)}}{E - E_H} + \frac{\psi_a^{(E_L)}\psi_b^{(E_L)}}{E - E_L} \quad (2)$$

where E_H and E_L are the energies of the HOMO and LUMO respectively. If the HOMO product $\psi_b^{(E_H)}\psi_a^{(E_H)}$ has the same sign as the LUMO product $\psi_b^{(E_L)}\psi_a^{(E_L)}$, then the right-hand side of eqn (2) will vanish at some energy E in the range $E_H \leqslant E \leqslant E_L$; that is, for some energy E within the HOMO–LUMO gap. In this case, one can say that the HOMO and the LUMO interfere destructively. On the other hand, if the HOMO and LUMO products have the opposite signs, then the right-hand side of eqn (2) will not vanish within the HOMO–LUMO gap and one can say that the HOMO and LUMO interfere constructively within the gap (they could have course interfere destructively at some other energy E outside the gap). When the right-hand side of eqn (2) vanishes, the main contribution to $g_{ba}(E)$ comes from all the other orbitals, so in general eqn (2) could be a poor approximation. One exception to this occurs when the lattice is bipartite, because the Coulson–Rushbrooke (CR) theorem[65] tells us that if a and b are both even or both odd, then the orbital products on the opposite sides of eqn (3) and (4) have the same sign. Consequently, when the HOMO and LUMO interfere destructively, all the other pairs of orbitals interfere destructively too, leading to the trivial zeros in the magic number table,[64] for which $g_{ba}(0) = 0$.

The equations of the Coulson–Rushbrooke (CR) theorem are denoted as:[65]

$$\psi_a^{(E_n)}\psi_b^{(E_n)} = \psi_a^{(-E_n)}\psi_b^{(-E_n)} \quad (3)$$

$$\psi_a^{(E_n)}\phi_b^{(E_n)} = \psi_a^{(-E_n)}\phi_b^{(-E_n)} \quad (4)$$

where $\psi_a^{(E_n)}$ is a vector of amplitudes on even-numbered sites, and $\phi_b^{(E_n)}$ is a vector of amplitudes on odd-numbered sites, $\pm E_n$

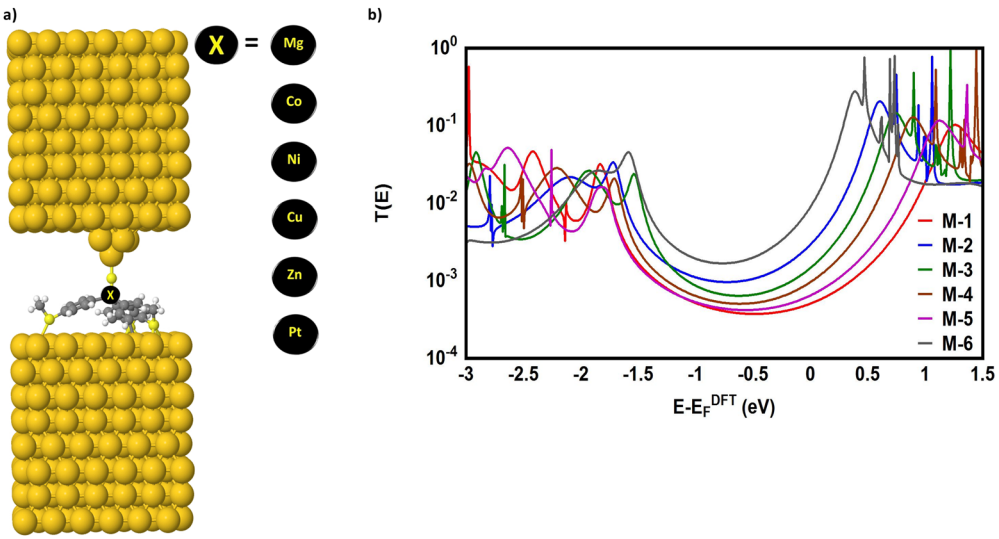

Fig. 2 (a) Theoretical model of molecular junctions; (b) transmission coefficient $T(E)$ as a function of electron energy for all molecules.

are eigenvalues that come in ± pairs, and the eigenstate belonging to $-E_n$ is related to the eigenstate belonging to E_n. Obviously, this exact cancellation is a property of bipartite lattices only, but based on its success for bipartite lattices, one might suppose that eqn (2) is a reasonable approximation for other lattices. Nevertheless, as pointed out by Yoshizawa *et al.*,[54,55,59,61] since orbitals such as those in Fig. 1(c) are often available from DFT calculations, it can be helpful to examine the question of whether or not the HOMO and LUMO (or indeed any other pair of orbitals) interfere destructively or constructively, by examining the colours of orbitals. This can be simplified by writing eqn (2) in the form below,

$$g_{ab}(E) \approx \frac{a_H}{E - E_H} + \frac{a_L}{E - E_L} \quad (5)$$

where $a_H = \psi_a^{(E_H)}\psi_b^{(E_H)}$ and $a_L = \psi_a^{(E_L)}\psi_b^{(E_L)}$. If the HOMO product a_H has the same sign as the LUMO product a_L, then the right-hand side of eqn (5) will vanish for some energy E in the range $E_H \leqslant E \leqslant E_L$. In other words, the HOMO and LUMO will interfere destructively at some energy within the HOMO–LUMO gap. However, this does not mean that the exact $g_{ba}(E)$ will vanish. Indeed, if the right-hand side of eqn (5) vanishes, then the contributions from all other orbitals become the dominant terms.[66] Nevertheless, this is an appealing method of identifying QI effects in molecules and describing their qualitative features. Now, based on this analysis, the results in Fig. 1(c) suggest that the transport behaviour is dominated by a constructive quantum interference phenomenon (CQI), since the product of the HOMO and LUMO amplitudes is the same (negative sign), which means that the HOMOs and LUMOs interfered constructively. These results are interpreting the high values of the transmission coefficient $T(E)$ shown in Table 1 and Fig. 2.

To support the results of the orbital analysis, and to confirm the impact of a constructive quantum interference (CQI), as well as to prove the important role of the different transition metals in improving the electronic and thermoelectric properties of tripod-based molecular junctions, a theoretical model of molecular junctions was constructed. This model was constructed using eight layers of (111)-oriented bulk gold, with each layer consisting of 6 × 6 atoms and a layer spacing of 0.235 nm, which were used to create the molecular junctions, as shown in Fig. 2(a) (see ESI† for all models). These layers were then further repeated to yield infinitely long current-carrying gold electrodes. Each molecule was attached to two (111)-directed gold electrodes; one of these electrodes was pyramidal, representing the scanning tunelling microscopy (STM) tip, while the other was a planar slab representing the electrode formed by the idealized Au(111) substrate in the I(s)-based molecular junction.[67–69] The molecules and first layers of the gold atoms within each electrode were then allowed to relax again, to yield the optimal junction geometries, as shown in Fig. 2(a) and Fig. S1 (ESI†). From these model junctions, the transmission coefficient, $T(E)$, was calculated using the GOLLUM code.[70]

The transmission coefficient according to Landauer–Büttiker[71] formalism is given by:

$$T(E) = T_r\{\Gamma_R(E)G^R(E)\Gamma_L(E)G^{R\dagger}(E)\} \quad (6)$$

where

$$\Gamma_{L,R}(E) = i(\Sigma_{L,R}(E) - \Sigma_{L,R}^{\dagger}(E)) \quad (7)$$

where $\Gamma_{L,R}$ describes the level broadening due to the coupling between the left (L) and right (R) electrodes and the central scattering region, and $\Sigma_{L,R}(E)$ are the retarded self-energies associated with this coupling. Also,

$$G^R = (E\chi - H - \Sigma_L - \Sigma_R)^{-1} \quad (8)$$

where G^R is the retarded Green's function, H is the Hamiltonian, and χ is the overlap matrix. The transport properties can then be calculated using the Landauer formula:

$$G = G_0 \int dE T(E)(-\partial f(E,T)/\partial E) \quad (9)$$

where $G_0 = 2e^2/h$ is the conductance quantum, $f(E) = (1 + \exp((E - E_F)/k_BT))^{-1}$ is the Fermi–Dirac distribution function, T is the temperature, and $k_B = 8.6 \times 10^{-5}$ eV K^{-1} is the Boltzmann's constant.

Fig. 2(a) shows the theoretical model of tripod-based molecular junctions with different metals (Mg, Co, Ni, Cu, Zn, and Pt). All the metals, except Mg, are d-block elements classified as transition metals. It is well known that magnesium does not have a d-orbital, while cobalt, nickel, and platinum atoms possess a partially filled d-orbital. The d-orbital is fully filled for copper and zinc atoms, as shown in Table 1. Regarding the relaxed geometries of the molecular junctions, it is obvious that while the thiolate (RS^-) to gold interaction has been studied extensively,[72,73] the methylthioether to gold interaction has been less thoroughly explored. Interestingly, all the compounds contact the flat gold surface *via* three SMe-anchor groups with an Au–S distance of 3.0 Å and an Au–S–C_{methyl} angle of 109.5°, as shown in Fig. 2(a). These geometries are comparable with other compounds, such as $[Ph_3PAuSMe_2]$–$[CF_3SO_3]$ (Au–S, 2.323(2) Å; Au–S–C_{methyl} 106.7(2), 104.7(2)°),[74] and as such the sulfur–gold interaction is well approximated in terms of a coordination-type interaction (chemisorption) between the sulfur donor atom of the thioether and the gold atom. Therefore, it is considered that Fig. 2(a) shows that the methyl thioether contacted compounds are not oriented normal to the idealized, flat electrode surface within the molecular junction. Rather,

Table 1 ($\Gamma = \Gamma_M - \Gamma_E$) is the number of transferred electrons from molecule to the electrodes; Γ_M is the number of electrons on the molecule in a gas phase; Γ_E is the number of electrons on the molecule in a junction; Π is number of electrons of the d-orbital; Ω (eV) is the gap between the highest occupied molecular orbitals (HOMO) and the lowest unoccupied molecular orbitals (LUMO); $T(E)$ is the transmission coefficient; LUMO is the lowest unoccupied molecular orbitals of all molecules in a junction

M	Metal	Γ	Π	Ω (eV)	$T(E)$
M-1	Mg	1.1	—	3.08	5.08×10^{-4}
M-2	Co	2.2	7	2.32	29.8×10^{-4}
M-3	Ni	1.8	8	2.27	14.8×10^{-4}
M-4	Cu	1.5	10	2.58	6.69×10^{-4}
M-5	Zn	1.3	10	2.94	6.5×10^{-4}
M-6	Pt	2.9	9	1.96	92×10^{-4}

they are tilted within molecular junctions to accommodate the directionality of the lone pairs of electrons on the sulfur atoms that bind to the gold electrodes,[75,76] which forces molecules to take a dome shape and contact the electrodes *via* all three legs. On the other hand, the thiolate-contacted groups sit close to the apex of each pyramid-shaped model gold electrode, with an Au–S distance of 2.5 Å and an Au–S–C_{ipso} angle of 177.7°.[77]

Fig. 2(b) shows the transmission coefficient $T(E)$ as a function of the electron energy for all the molecular junctions. All the molecular junctions show a high value of $T(E)$, ranging from the lowest value for molecule M-1 (5.08×10^{-4}) to the highest value for molecule M-6 (92×10^{-4}), as shown in Table 1. These results are reflective of constructive quantum interference (CQI), consistent with ref. 78–91, and the LUMO states of all molecules are near the theoretical Fermi level (0.0 eV), which suggests a LUMO-transport mechanism, which is in excellent agreement with the predicted outcomes from the orbital analysis calculations. The transmission values obtained from the M-4 and M-5 systems were close to each other, suggesting that the readily synthesized copper and zinc complexes may have an important role to play in the further development of metal complexes for applications in single-molecule electronics. These metal complexes are more conductive than their purely organic analogues of comparable molecular length,[5] as shown in Fig. 3. To prove the important role of the d-orbitals in improving the electrical conductance (G/G_0), the results shown in Fig. 3 are quoted from our previous study.[5] Fig. 3 shows a comparison between the calculated G/G_0 for organometallic connectors and the measured G/G_0 for organic molecules.

It can also be see in Fig. 3 that the experimental break-off distance (Z^*) of all the organic-molecular junctions was smaller than the calculated electrode separation (Z) of the organometallic-molecular junctions. However, the values of the (G/G_0) of the molecules with transition metals (Theory) were higher than those of the organic molecules (Expermint). These results could be interpreted in terms of the signature of the d-orbitals, which increase the electrical conductance. In addition, these results demonstred that all three-connector molecules (organic and organometallic molecules) had high electrical conductance, which could be ascribed to the high junction-formation probability due to the high binding energy between the three legs and gold electrodes.[5]

Furthermore, it is well known that the electrical conductance decreases with increasing the tunnelling distance.[92] The molecule length of all the molecules was consistent with a dominant contribution from a coherent tunnelling mechanism.[93–97] The rectangular tunnel barrier model[98] states that the electrical conductance through a single molecule (barrier) decreases exponentially with the length of the barrier, according to the following equation:

$$T(E) \propto e^{-\beta l} \quad (10)$$

where $T(E)$ is the transmission coefficient, β is the electronic decay constant, and l is the tunnelling distance. Herein, the organometallic molecules (Theory) represented the longest

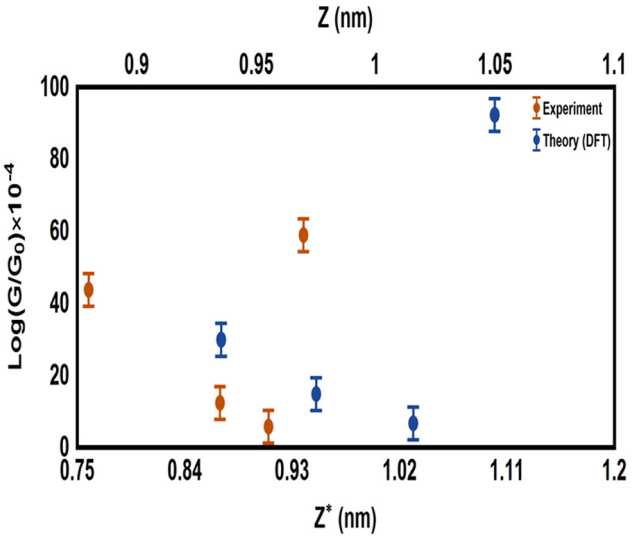

Fig. 3 Comparison between the calculated electrical conductance (G/G_0) of the organometallic molecules in the current investigation, and the measured G/G_0 of organic molecules from our previous studies.[5] The experimental results have been adapted with permission from ref. 5. Copyright 2018 Royal Society of Chemistry. $Exper_{G/G_0}$ is a function of the experimental break-off distance (Z^*), while the theoretical electrical conductance ($Theore_{G/G_0}$) is a function of the calculated electrode separation in relaxed junctions (Z); $Z = d_{Au-Au} - 0.25$ nm, where 0.25 nm is the calculated centre-to-centre distance of the apex atoms of the two opposing gold electrodes when the conductance = G_0 in the absence of the molecule.

molecules, but they showed the highest value of $T(E)$. In contrast, the organic (Experiment) molecules represented the shortest length, but they showed transmission values that were several-fold lower than that of organometallic molecules, as shown in Fig. 3. Hence, it became clear that there was competition between two parameters, the first one is the tunnelling distance and the second is the presence of the d-orbital effect. These results showed that the existence of the impact of transition metals was dominant, which led to the distinctive difference in the electrical conductance values between the experimental and theoretical results. On the other hand, the partial charge transfer (Γ), as shown in Table 1 and Fig. 4(a), may also be responsible for the high transmission coefficient values presented in Table 1 and Fig. 2(b). Thygesen *et al.*[89] discussed similar situations for C_{60}-contacted molecular wires and showed that critical molecular orbitals can become pinned close to the Fermi level due to partial charge transfer, leading to a high electrical conductance.[90] In addition, Fig. 4(a) illustrates the relationship between the number of transffered electrons from the molecule to the gold electrodes (Γ) and the HOMO–LUMO (H–L) gap (Ω) eV of the molecules in a junction. Overall, the energy levels moved energetically downwards and the H–L gap shrank for all the molecules with transition metals. The values of the H–L gaps for the M-5, M-4, M-2, and M-3 molecules were 2.94, 2.58, 2.32, and 2.27 eV respectively, as shown in Table 1. Interestingly, Fig. 4(a) presents an important result indicating that the molecule offering the highest number of transferred electrons (Γ) showed the narrowest energy gap,

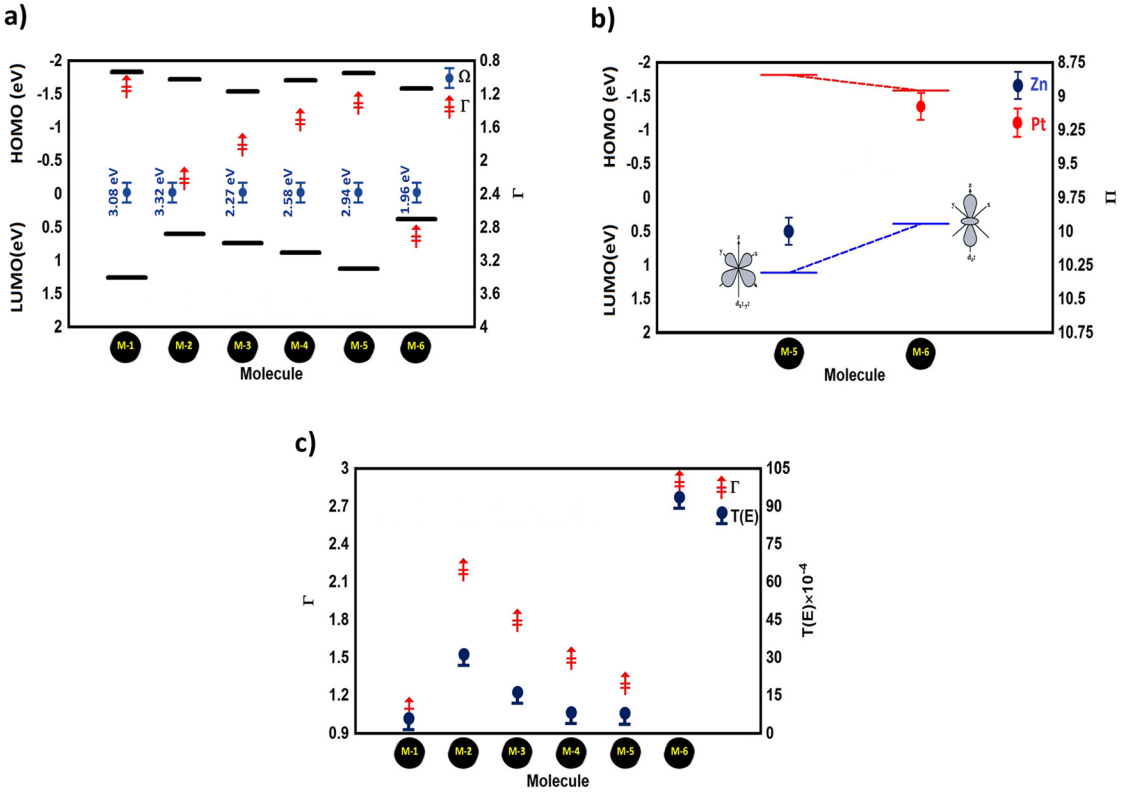

Fig. 4 (a) HOMO–LUMO gap (Ω) *versus* the number of transferred electrons (Γ) of the molecular junctions; (b) orbital energies *versus* the number of electrons in the d-orbital (Π) for M-5 and M-6 molecules, as example system with even and odd numbers of electrons; (c) number of transferred electrons from the molecule to the electrodes (Γ) *versus* the transmission coefficient $T(E)$ of all the molecular junctions.

and *vice versa*, since molecule M-6 offering the highest number of transferred electrons (2.9 electrons) exhibted the narrowest H–L gap (1.96 eV). In contrast, molecule M-1 introduced the lowest Γ of 1.1 electrons, and the widest H–L gap of 3.08 eV. Now, we sought to obtain a deep understanding of this finding and to answer the question of what is the relationship between Γ and Ω. This work considered the relation between the even and odd numbers of electrons in the d-orbitals (Π). The orientations of these orbitals and the HOMO–LUMO gap (Ω) for Zn- and Pt-based molelecular junctions were considered as example of even and odd cases, as shown in Fig. 4(b). The picture of these results could be understood according to the crystal field theory (CFT) concept.[55] Here, the LUMO energies of the two d-orbitals groups ($d_{x^2-y^2}$ and d_{z^2}) for M-5 and M-6, respectively, depend on their orientations. The d_{z^2} orbital has a dumbbell form with a doughnut-shaped electron cloud in the centre and is symmetrical about the Z-axis. The value of the HOMO–LUMO (H–L) gap of this orbital is 0.38 eV, which represents the narrowest gap. In contrast, the $d_{x^2-y^2}$ orbital is likewise in the shape of a clover leaf, but its leaves are oriented along the X and Y axes. The H–L gap value of this orbital is 2.94 eV, which is wider than that of the d_{z^2} orbital. This brings us to a predication that an odd number of electrons results in a narrow gap, while an even number leads to a wide one. On the other hand, the quantum-chemical electronic structure analysis shown in Fig. 4(b) indicates that such a metal–carbon interaction is a positive dπ–pπ hyperconjugation, which in turn increases the conjugation of the Pt-based molecular junction (M-6), resulting in its highest value of Γ,[59] and the latter increased $T(E)$, as shown in Fig. 4(c). The value of the transmission coefficient $T(E)$ of the Zn-based molecular junction (M-5) was lower than that of the Pt-based molecular junction (M-6). The order of $T(E)$ for all the molecular junctions is $T(E)_{M\text{-}6} > T(E)_{M\text{-}2} > T(E)_{M\text{-}3} > T(E)_{M\text{-}4} > T(E)_{M\text{-}5} > T(E)_{M\text{-}1}$.

Exploring the influence of CQI on the transport behaviour, and consequently on the thermoelectric properties was one of the main goals of this work. The slope of $T(E)$ determines the Seebeck coefficient (S), and thus the electronic figure of merit ($Z_{el}T$). The Seebeck coefficient (S), power factor (P), and ($Z_{el}T$), are given by:

$$S \approx -L|e|T\left(\frac{\mathrm{d}\ln\ T(E)}{\mathrm{d}E}\right)_{E=E_F} \tag{11}$$

where L is the Lorenz number $L = \left(\frac{k_B}{e}\right)^2\frac{\pi^2}{3} = 2.44 \times 10^{-8}$ W Ω K^{-2}. In other words, S is proportional to the negative of the slope of $\ln T(E)$, evaluated at the Fermi energy (0.0 eV). Based on the Seebeck coefficient, the power factor (P) is calculated by:

$$P = GS^2T \tag{12}$$

where T is the temperature T = 300 K, G is the electrical conductance and S is the Seebeck coefficient, and the purely electronic figure of merit ($Z_{el}T$) is given by:[91]

$$Z_{el}T = \frac{S^2 G}{k_{el}}T = \frac{S^2}{L} \quad (13)$$

where k_{el} is the electron thermal conductance. According to previous studies,[91,99] the figure of merit in this work has been calculated only based on a purely electronic contribution. Indeed, it is well known that the performance of thermoelectric materials is characterized by an efficient conversion of an input heat to electricity.[100,101] In this context, the enhancement of the power factor (P) and electronic figure of merit ($Z_{el}T$), which depend on the Seebeck coefficient (S), are important too.

Fig. 5(a), (b) and Table 2 show that the highest values of S, $Z_{el}T$, and P (−43.2 μV K^{-1}, 0.068, and 1330.629 W K^{-1} × 10^{-15}, respectively) were exhibited by molecule M-6. In contrast, molecule M-1 presented the lowest values (−9.9 μV K^{-1}, 0.004, and 0.392 W K^{-1} × 10^{-15}). For M-2, M-3, M-4, and M-5 molecules, the molecule (M-2) with a Co metal centre possessing an odd number of electrons in its d-orbital showed values of S and $Z_{el}T$ higher than those of the transition metals with an even number of electrons in their d-orbitals, as shown in Table 2. These results could be ascribed to the metal–carbon dπ–pπ hyperconjugation due to the odd number of electrons in the d-orbitals, which modulate the transmission behaviour of single-molecule junctions, as shown in Fig. 6. In addition, the competition between the electrical conductance and Seebeck coefficient according to eqn (12) led to power factors for the molecules in the order of $P_{M\text{-}6} > P_{M\text{-}3} > P_{M\text{-}4} > P_{M\text{-}5} > P_{M\text{-}1}$.

Table 2 Seebeck coefficient (S); electrical conductance (G); power factor (P); electronic figure of merit ($Z_{el}T$); and threshold voltage (V_{th}) of all the molecular junctions

M	S (μK V^{-1})	G (S × 10^{-7})	P (W K^{-1} × 10^{-15})	$Z_{el}T$	V_{th} (V)
M-1	−9.9	0.4	0.392	0.004	0.95
M-2	−26.7	2.3	16.396	0.028	0.33
M-3	−21.5	1.14	52.696	0.018	0.45
M-4	−16.9	0.76	21.706	0.011	0.65
M-5	−12.2	0.5	7.442	0.006	0.7
M-6	−43.2	7.13	1330.629	0.068	0.15

In light of the aforementioned results, it is clear that the transition-metal-based molecules could be considered promising candidates for thermoelectric applications. Obviously, the Seebeck coefficient was negative, which was consistent with the transport behaviour and the orbital analysis indicating that the transport mechanism was LUMO-dominated. Furthermore, Fig. 5(c) and Table 2 present the current–voltage (I–V) characteristics of all the molecular junctions, which were limited to the first and third quadrants of the I–V plane crossing the origin. Therefore, they could be classified as components that consume the electric power, and here the importance of the threshold voltage (V_{th}) value appears. The values of V_{th} ranged from 0.15 to 0.95 V. In general, the I–V characteristics of all the molecular junctions exhibited a semiconductor behaviour. Importantly, the values of V_{th} for molecules M-6, M-2, and

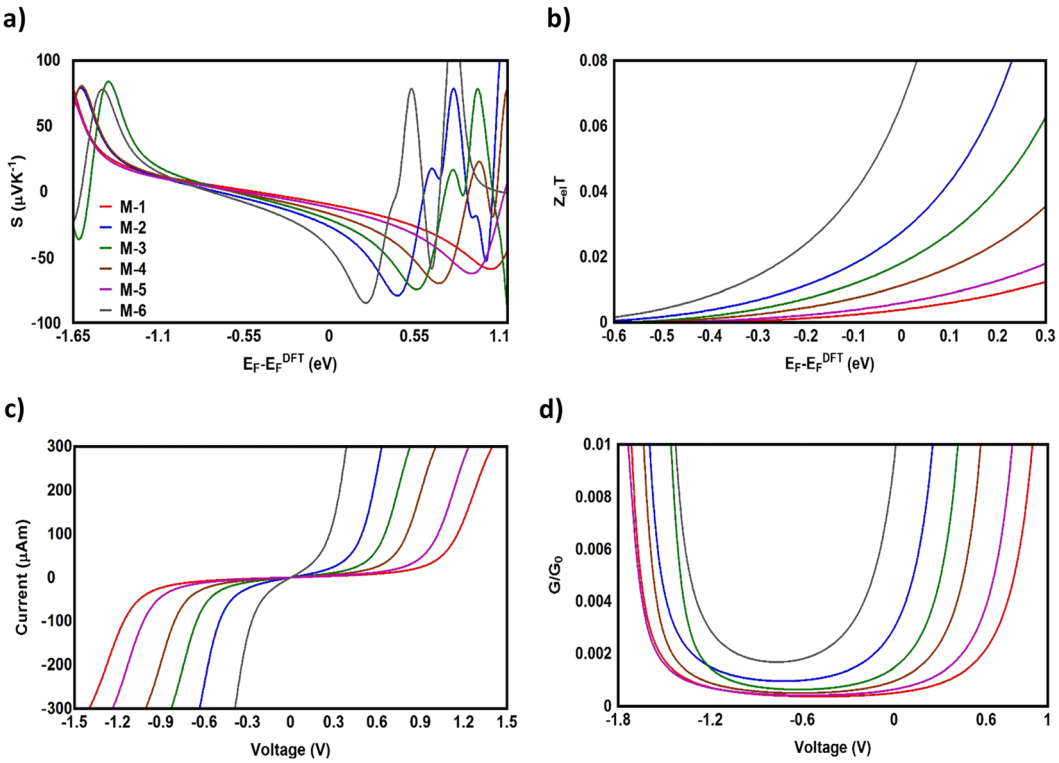

Fig. 5 (a) Seebeck coefficient (S); (b) electronic figure of merit ($Z_{el}T$), as a function of the Fermi energy; (c) current–voltage characteristics; (d) electrical conductance (G/G_0) as a function of voltage for all the molecular junctions.

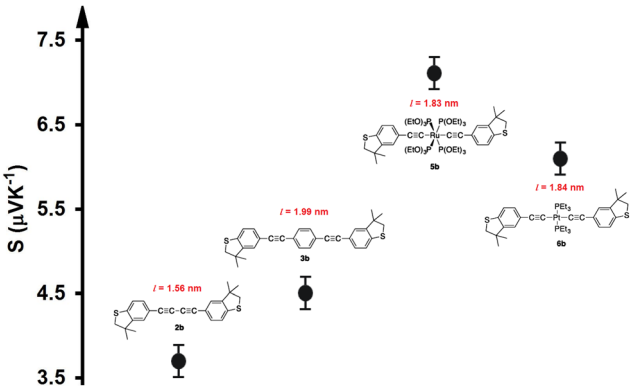

Fig. 6 Experimental thermopower results for previously studied compounds.[34] The data were adapted with permission from ref. 34. Copyright 2015 American Chemical Society.

M-3 were 0.15, 0.33, and 0.45 V, which are all below 0.5 V, indicating that these molecules are suitable structures for electronic applications.[102] These results show a clear message that partially occupied d-orbitals may be an important property in improving the electronic and thermoelectric properties of transition-metal based molecular junctions.[103] Moreover, as the voltage increased, the density of electrons also increased, which led to an increase in the number of occupied sub-bands,[104] which in turn increased the conductance (in G/G_0), as shown in Fig. 5(d). The most prominent result depicted in Fig. 6 is that the values of the thermoelectric properties (S and $Z_{el}T$) of the transition-metal-based molecular junctions were higher than those based on non-transition metals. On the other hand, Fig. 6 proves that the molecules with metals involved dumbbell-form d-orbitals and had S and $Z_{el}T$ values higher than that of molecules with d-orbitals with a clover-leaf shape. Significantly, these results demonstrate that the existence of the transition metals centre improves the thermoelectric properties of the system.[105]

To validate and support the predictions of the current investigation regarding the thermoelectric signature of d-orbitals, we adopted some of the experimental results of our previous study.[34] Fig. 6 shows the Seebeck coefficient of four molecules, two of them (5b and 6b) involved transition metals (Ru and Pt) as metal centres, while the other molecules (2b and 3b) were organic. The data were adapted with permission from ref. 34. Copyright 2015 American Chemical Society. Despite, the length of molecule 2b (1.56 nm) being shorter than that of molecule 5b (1.83 nm), and the lengths of molecules 3b and 6b (1.99 and 1.84 nm respectively) being somewhat identical, Fig. 6 demonstrates that the highest values (7.1 and 6.1 μV K^{-1}) of Seebeck coefficient were exhibited by the organometallic molecules 5b and 6b, respectively. Furthermore, when two points of the conductor are maintained at different temperatures, electrons or holes in the hotter region will move towards the colder region and diffuse. This diffusion stops when the electric field generated due to the migration of charges has established a strong field. For a metal, with carriers being negatively charged electrons, the colder end would become negative, so that the Seebeck coefficient would be negative. In a p-type semiconductor, holes diffuse towards the lower temperature, resulting in a positive Seebeck coefficient. These results leave us with only one explanation, which is that the presence of transition metals significantly improved the thermoelectric properties of the single-molecule junctions.

Conclusions

In summary, this work reports an investigation of the thermoelectric properties of molecular junctions based on tripod connectors terminated by active functional groups (SMe). The considerable and negative values of the Seebeck coefficient established that transport through these molecules took place by tunnelling through the tail of the LUMO resonance near the middle of the HOMO–LUMO gap. The results of this work prove that the tripod template significantly improves the junction-formation probability for increasing the electrical conductance. The excellent consistency between the current theoretical results and experimental outcomes of previous studies demonstrates the important role of transition metals in improving the thermoelectric properties of molecular junctions. In the case of the cobalt and platinum compounds M-2 and M-6, the odd number of electrons in their d-orbitals showed a robust signature in enhancing the Seebeck coefficient, making them to be promising candidates for thermoelectric applications.

Computational methods

Initial optimization of the gas-phase molecules and charges population analysis[60] were carried out at the B3LYP level of theory[56] with the LANL2DZ basis set.[57,58] Geometrical optimization of the gold|molecule|gold configurations under investigation in this work was achieved by implementation of DFT[106,107] in the SIESTA[106] code, as shown in Fig. S2 (see ESI†). The generalized gradient approximation (GGA) of the exchange and correlation functional was used with a double-ζ polarized (DZP) basis set, a real-space grid defined with an equivalent energy cut-off of 250 Ry. The geometry optimization for each structure was performed for forces smaller than 20 meV $Å^{-1}$. The mean-field Hamiltonian obtained from the converged DFT calculations was combined with GOLLUM[70] code. The quantum transport theory (QTT)[45–48,56,57,60,106] implemented in GOLLUM was used to calculate the electronic and thermoelectric properties of all the molecular junctions.

Data availability

The data are available in the manuscript and ESI.†

Conflicts of interest

The authors declare no conflict of interest.

Acknowledgements

O. A. A. and H. N. N. give a deep thanks and appreciation to the University of Babylon for the support. O. A. A.; A. K. O. A.; N. H. A.; M. S. A.; M. H. D. and M. A. A. express their sincere thanks and gratitude to the Al-Zahrawi University College and the University of Karbala for their kind support. A. K. O. A. thanks Al-Qasim Green University for the support.

References

1 N. J. Tao, *Nat. Nanotechnol.*, 2006, **1**, 173–181.
2 S. S. Alexandre, J. M. Soler, P. J. Sanz Miguel, R. W. Nunes, F. Yndurain, J. Gómez-Herrero and F. Zamora, *Appl. Phys. Lett.*, 2007, **90**, 193107.
3 W. Hong, D. Z. Manrique, P. Moreno-García, M. Gulcur, A. Mishchenko, C. J. Lambert, M. R. Bryce and T. Wandlowski, *J. Am. Chem. Soc.*, 2012, **134**, 2292–2304.
4 V. Kaliginedi, A. V. Rudnev, P. Moreno-Garcia, M. Baghernejad, C. Huang, W. Hong and T. Wandlowski, *Phys. Chem. Chem. Phys.*, 2014, **16**, 23529–23539.
5 R. J. Davidson, D. C. Milan, O. A. Al-Owaedi, A. K. Ismael, R. J. Nichols, S. J. Higgins, C. J. Lambert, D. S. Yufita and A. Beeby, *RSC Adv.*, 2018, **8**, 23585–23590.
6 J. K. Whitesell and H. K. Chang, *Science*, 1993, **261**, 73–76.
7 M. A. Fox, J. K. Whitesell and A. J. McKerrow, *Langmuir*, 1998, **14**, 816–820.
8 Y. Yao and J. M. Tour, *J. Org. Chem.*, 1999, **64**, 1968–1971.
9 W. Guo, E. Galoppini, G. Rydja and G. Pardi, *Tetrahedron Lett.*, 2000, **41**, 7419–7421.
10 E. Galoppini, W. Guo, P. Qu and G. J. Meyer, *J. Am. Chem. Soc.*, 2001, **123**, 4342–4343.
11 E. Galoppini, W. Guo, W. Zhang, P. G. Hoertz, P. Qu and G. J. Meyer, *J. Am. Chem. Soc.*, 2002, **124**, 7801–7811.
12 X. Deng and C. Cai, *Tetrahedron Lett.*, 2003, **44**, 815–817.
13 R. S. Loewe, A. Ambroise, K. Muthukumaran, K. Padmaja, A. B. Lysenko, G. Mathur, Q. Li, D. F. Bocian, V. Misra and J. S. Lindsey, *J. Org. Chem.*, 2004, **69**, 1453–1460.
14 L. Zhu, H. Tang, Y. Harima, K. Yamashita, D. Hirayama, Y. Aso and T. Otsubo, *Chem. Commun.*, 2001, 1830–1831.
15 D. Hirayama, K. Takimiya, Y. Aso, T. Otsubo, T. Hasobe, H. Yamada, H. Imahori, S. Fukuzumi and Y. Sakata, *J. Am. Chem. Soc.*, 2002, **124**, 532–533.
16 O. A. Al-Owaedi, *RSC Adv.*, 2024, **14**, 14704–14715.
17 L. Wei, K. Padmaja, W. J. Youngblood, A. B. Lysenko, J. S. Lindsey and D. F. Bocian, *J. Org. Chem.*, 2004, **69**, 1461–1469.
18 L. Wei, H. Tiznado, G. Liu, K. Padmaja, J. S. Lindsey, F. Zaera and D. F. Roclan, *J. Phys. Chem. B*, 2005, **109**, 23963–23971.
19 Y. Ie, T. Hirose, A. Yao, T. Yamada, N. Takagi, M. Kawai and Y. Aso, *Phys. Chem. Chem. Phys.*, 2009, **11**, 4949–4951.
20 M. A. Karimi, S. G. Bahoosh, M. Valasek, M. Burkle, M. Mayor, F. Pauly and E. Scheer, *Nanoscale*, 2016, **8**, 10582–10590.
21 B. Xu and N. J. Tao, *Science*, 2003, **301**, 1221–1223.
22 M. Valasek, M. Lindner and M. Mayor, *Beilstein J. Nanotechnol.*, 2016, **7**, 374–405.
23 Y. Ie, T. Hirose, H. Nakamura, M. Kiguchi, N. Takagi, M. Kawai and Y. Aso, *J. Am. Chem. Soc.*, 2011, **133**, 3014–3022.
24 L. Gerhard, K. Edelmann, J. Homberg, M. Valasek, S. G. Bahoosh, M. Lukas, F. Pauly, M. Mayor and W. Wulfekel, *Nat. Commun.*, 2017, **8**, 14672.
25 O. A. Al-Owaedi, D. C. Milan, M. Oerthel, S. Bock, D. S. Yufit, J. A. K. Howard, S. J. Higgins, R. J. Nichols, C. J. Lambert, M. R. Bryce and P. J. Low, *Organometallics*, 2016, **35**, 2944–2954.
26 O. A. Al-Owaedi, *ChemPhysChem*, 2024, **25**, e202300616.
27 A. A. Al-Jobory and M. D. Noori, *J. Electron. Mater.*, 2020, **49**, 5455–5459.
28 M. Alsaqer, A. H. S. Daaoub, S. Sangtarash and H. Sadeghi, *Nano Lett.*, 2023, **23**, 10719–10724.
29 Z. Liu, T. Liu, C. N. Savory, J. P. Jurado, J. S. Reparaz, J. Li, L. Pan, C. F. J. Faul, I. P. Parkin, G. Sankar, S. Matsuishi, M. Campoy-Quiles, D. O. Scanlon, M. A. Zwijnenburg, O. Fenwick and B. C. Schroeder, *Adv. Funct. Mater.*, 2020, **30**, 2003106.
30 H. Ozawa, M. Baghernejad, O. A. Al-Owaedi, V. Kaliginedi, T. Nagashima, J. Ferrer, T. Wandlowski, V. M. Garcia-Suarez, P. Broekmann, C. J. Lambert and M. Haga, *Chem. – Eur. J.*, 2016, **22**, 12732–12740.
31 S. Bock, O. A. Al-Owaedi, S. G. Eaves, D. C. Milan, M. Lemmer, B. W. Skelton, H. M. Osorio, R. J. Nichols, S. J. Higgins, P. Cea, N. J. Long, T. Albrecht, S. Martin, C. J. Lambert and P. J. Low, *Chem. – Eur. J.*, 2017, **23**, 2133–2143.
32 G. Lovat, B. Choi, D. W. Paley, M. L. Steigerwald, L. Venkataraman and X. Roy, *Nat. Nanotechnol.*, 2017, **12**, 1050–1054.
33 S. Gunasekaran, D. A. Reed, D. W. Paley, A. K. Bartholomew, L. Venkataraman, M. L. Steigerwald, X. Roy and C. Nuckolls, *J. Am. Chem. Soc.*, 2020, **142**, 14924–14932.
34 M. Naher, D. C. Milan, O. A. Al-Owaedi, I. J. Planje, S. Bock, J. Hurtado-Gallego, P. Bastante, Z. M. Abd Dawood, L. RinconGarcia, G. Rubio-Bollinger, S. J. Higgins, N. Agrait, C. J. Lambert, R. J. Nichols and P. J. Low, *J. Am. Chem. Soc.*, 2021, **143**, 3817–3829.
35 P. Gehring, J. K. Sowa, C. Hsu, J. de Bruijckere, M. van der Star, J. J. Le Roy, L. Bogani, E. M. Gauger and H. S. J. van der Zant, *Nat. Nanotechnol.*, 2021, **16**, 426–430.
36 F. Schwarz, G. Kastlunger, F. Lissel, C. Egler-Lucas, S. N. Semenov, K. Venkatesan, H. Berke, R. Stadler and E. Lortscher, *Nat. Nanotechnol.*, 2016, **11**, 170–176.
37 E. Coronado and A. J. Epsetin, *J. Mater. Chem.*, 2009, **19**, 1670–1671.
38 T. Albrecht, A. Guckian, J. Ulstrup and J. G. Vos, *Nano Lett.*, 2005, **5**, 1451–1455.
39 X. Xiao, D. Brune, J. He, S. Lindsay, C. B. Gorman and N. Tao, *Chem. Phys.*, 2006, **326**, 138–143.
40 S. Mori and M. Shindo, *Org. Lett.*, 2004, **6**, 3945–3948.

41 A. G. Davies, *J. Chem. Soc., Perkin Trans. 2*, 1999, 2461–2467.
42 K. Xiao, Y. Zhao, J. Zhu and L. Zhao, *Nat. Commun.*, 2019, **10**, 5639.
43 D. V. Vidhani, M. E. Krafft and I. V. Alabugin, *J. Am. Chem. Soc.*, 2016, **138**, 2769–2779.
44 J. Yuan, T. Sun, X. He, K. An, J. Zhu and L. Zhao, *Nat. Commun.*, 2016, **7**, 11489.
45 H. T. Liu, X. G. Xiong, P. Diem Dau, Y.-L. Wang, D.-L. Huang, J. Li and L.-S. Wang, *Nat. Commun.*, 2013, **4**, 2223.
46 J. Dong, J. R. Robinson, Z.-H. Gao and L.-S. Wang, *J. Am. Chem. Soc.*, 2022, **144**, 12501–12509.
47 M. A. Esteruelas, A. M. López and M. Oliván, *Chem. Rev.*, 2016, **116**, 8770–8847.
48 Q. Zhuo, J. Lin, Y. Hua, X. Zhou, Y. Shao, S. Chen, Z. Chen, J. Zhu, H. Zhang and H. Xia, *Nat. Commun.*, 2017, **8**, 1912.
49 M. Lukas, K. Dössel, A. Schramm, O. Fuhr, C. Stroh, M. Mayor, K. Fink and H. V. Löhneysen, *ACS Nano*, 2013, **7**, 6170–6180.
50 S. Katano, Y. Kim, H. Matsubara, T. Kitagawa and M. Kawai, *J. Am. Chem. Soc.*, 2007, **129**, 2511–2515.
51 F. L. Otte, S. C. Lemke, S. N. R. Krekiehn, U. J. O. M. Magnussen and R. Herges, *J. Am. Chem. Soc.*, 2014, **136**, 11248–11251.
52 Y. Ie, K. Tanaka, A. Tashiro, S. K. Lee, H. R. Testai, R. Yamada, H. Tada and Y. Aso, *J. Phys. Chem. Lett.*, 2015, **6**, 3754–3759.
53 T. Kitagawa, Y. Idomoto, H. Matsubara, D. Hobara, T. Kakiuchi, T. Okazaki and K. Komatsu, *J. Org. Chem.*, 2006, **71**, 1362–1369.
54 J. M. Parr, A. J. P. Whitea and M. R. Crimmin, *Chem. Sci.*, 2022, **13**, 6592–6598.
55 H. Bethe, *Ann. Phys.*, 1929, **395**, 133–208.
56 A. D. Becke, *J. Chem. Phys.*, 1993, **98**, 5648–5652.
57 G. A. Petersson, A. Bennett, T. G. Tensfeldt, M. Al-Laham, W. A. Shirley and J. Mantzaris, A complete basis set model, *J. Chem. Phys.*, 1988, **89**, 2193–2198.
58 G. A. Petersson and M. A. Al-Laham, *J. Chem. Phys.*, 1991, **94**, 6081–6090.
59 O. A. Al-Owaedi, S. Bock, D. C. Milan, M. Oerthel, M. S. Inkpen, D. S. Yufit, A. N. Sobolev, N. J. Long, T. Albrecht, S. J. Higgins, M. R. Bryce, R. J. Nichols, C. J. Lambert and P. J. Low, *Nanoscale*, 2017, **9**, 9902–9912.
60 R. S. Mulliken, *J. Chem. Phys.*, 1955, **23**, 1833–1840.
61 T. Albrecht, A. Guckian, A. M. Kuznetsov, J. G. Vos and J. Ulstrup, *J. Am. Chem. Soc.*, 2006, **128**, 17132–17138.
62 V. P. Georgiev and J. E. McGrady, *J. Am. Chem. Soc.*, 2011, **133**, 12590–12599.
63 C. J. Lambert, *Quantum Transport in Nanostructures and Molecules*, IOP Publishing Ltd, 2021.
64 C. J. Lambert and S.-X. Liu, *Chem. – Eur. J.*, 2018, **24**, 4193–4201.
65 C. A. Coulson and G. S. Rushbrooke, *Math. Proc. Cambridge Philos. Soc.*, 1940, **36**, 193–200.
66 M. Camarasa-Gómez, D. Hernangómez-Pérez, M. S. G. Inkpen, E. Lovat, E. Fung, X. Roy, L. Venkataraman and F. Evers, *Nano Lett.*, 2020, **20**, 6381–6386.
67 W. Haiss, R. J. Nichols, H. Van Zalinge, S. J. Higgins, D. Bethell and D. J. Schiffrin, *Phys. Chem. Chem. Phys.*, 2004, **6**, 4330–4337.
68 W. Haiss, H. Van Zalinge, S. J. Higgins, D. Bethell, H. Hobenreich, D. J. Schiffrin and R. J. Nichols, *J. Am. Chem. Soc.*, 2003, **125**, 15294–15295.
69 R. J. Nichols, W. Haiss, S. J. Higgins, E. Leary, S. Martin and D. Bethell, *Phys. Chem. Chem. Phys.*, 2010, **12**, 2801–2815.
70 J. Ferrer, C. J. Lambert, V. M. García-Suárez, D. Zs Manrique, D. Visontai, L. Oroszlany, R. Rodríguez-Ferradás, I. Grace, S. W. D. Bailey, K. Gillemot, H. Sadeghi and L. A. Algharagholy, *New J. Phys.*, 2014, **16**, 93029.
71 M. Büttiker and R. Landauer, *Phys. Rev. Lett.*, 1982, **49**, 1739–1742.
72 H. Hakkinen, *Nat. Chem.*, 2012, **4**, 443–455.
73 C. Herrmann, G. C. Solomon and M. A. Ratner, *J. Phys. Chem. C*, 2010, **114**, 20813–20820.
74 J. M. López-De-Luzuriaga, A. Schier and H. Schmidbaur, *Chem. Ber. lRecueil*, 1997, **130**, 647–650.
75 B. Capozzi, E. J. Dell, T. C. Berkelbach, D. R. Reichman, L. Venkataraman and L. M. Campos, *J. Am. Chem. Soc.*, 2014, **136**, 10486–10492.
76 H. Häkkinen, *Nat. Chem.*, 2012, **4**, 443–455.
77 A. S. Mikherdov, M. Jin and H. Ito, *Chem. Sci.*, 2023, **14**, 4485–4494.
78 J. Liu, X. Huang, F. Wang and W. Hong, *Acc. Chem. Res.*, 2019, **52**, 151–160.
79 C. Nappi, F. Romeo, L. Parlato, F. D. Capua, A. Aloisio and E. Sarnelli, *J. Phys. Chem. C*, 2018, **122**, 11498–11504.
80 J. P. Bergfield, G. C. Solomon, C. A. Stafford and M. A. Ratner, *Nano Lett.*, 2011, **11**, 2759–2764.
81 O. A. Al-Owaedi, *ACS Omega*, 2024, **9**, 10610–10620.
82 L. Huang, Y. Su and C. Kaun, *ACS Omega*, 2018, **3**, 9191–9195.
83 G. Gryn'ova and C. Corminboeuf, *J. Phys. Chem. Lett.*, 2019, **10**, 825–830.
84 D. Z. Manrique, C. Huang, M. Baghernejad, X. Zhao, O. A. Al-Owaedi, H. Sadeghi, V. Kaliginedi, W. Hong, M. Gulcur, T. Wandlowski, R. M. Bryce and C. J. Lambert, *Nat. Commun.*, 2015, **6**, 6389.
85 S. Li, H. Yu, K. Schwieter, K. Chen, B. Li, Y. Liu, J. S. Moore and C. M. Schroeder, *J. Am. Chem. Soc.*, 2019, **141**, 16079–16084.
86 O. A. Al-Owaedi, T. T. Khalil, S. A. Karim, E. Al-Bermany and D. N. Taha, *Syst. Rev. Pharm.*, 2020, **11**, 110–115.
87 H. Ozawa, M. Baghernejad, O. A. Al-Owaedi, V. Kaliginedi, T. Nagashima, J. Ferrer, T. Wandlowski, V. M. García-Suárez, P. Broekmann, C. J. Lambert and M. Haga, *Chem. – Eur. J.*, 2016, **22**, 12732–12740.
88 M. A. I. Obayes, E. M. Al-Robayi and O. A. Al-Owaedi, *J. Phys.: Conf. Ser.*, 2021, **1973**, 012147.
89 T. Markussen, M. Settnes and K. S. Thygesen, *J. Chem. Phys.*, 2011, **135**, 144104.
90 N. Cao, W. Bro-Jørgensen, X. Zheng and G. C. Solomon, *J. Chem. Phys.*, 2023, **158**, 124305.

91 M. Burkle, T. J. Hellmuth, F. Pauly and Y. Asai, *Phys. Rev. B: Condens. Matter Mater. Phys.*, 2015, **91**, 165419.
92 S. H. Halboos, O. A. Al-Owaedi and E. M. Al-Robayia, *Nanoscale Adv.*, 2024, **6**, 5467–5481.
93 F. Jiang, D. I. Trupp, N. Algethami, H. Zheng, W. He, A. Alqorashi, C. Zhu, C. Tang, R. Li, J. Liu, H. Sadeghi, J. Shi, R. Davidson, M. Korb, A. N. Sobolev, M. Naher, S. Sangtarash, P. J. Low, W. Hong and C. J. Lambert, *Angew. Chem., Int. Ed.*, 2019, **58**, 18987–18993.
94 M. H. Garner, H. X. Li, Y. Chen, T. A. Su, Z. Shangguan, D. W. Paley, T. F. Liu, F. Ng, H. X. Li, S. X. Xiao, C. Nuckolls, L. Venkataraman and G. C. Solomon, *Nature*, 2018, **558**, 415–419.
95 B. Huang, X. Liu, Y. Yuan, Z. Hong, J. Zheng, L. Pei, Y. Shao, J. Li, X. Zhou, J. Chen, S. Jin and B. Mao, *J. Am. Chem. Soc.*, 2018, **140**, 17685–17690.
96 B. Kim, J. M. Beebe, C. Olivier, S. Rigaut, D. Touchard, J. G. Kushmerick, X. Y. Zhu and C. D. Frisbie, *J. Phys. Chem. C*, 2007, **111**, 7521–7526.
97 S. M. S. Al-Mohana, H. N. Najeeb, R. M. Al-Utayjawee, F. Babaeia and O. A. Al-Owaedi, *RSC Adv.*, 2024, **14**, 23699–23709.
98 Q. Lu, K. Liu, H. M. Zhang, Z. B. Du, X. H. Wang and F. S. Wang, *ACS Nano*, 2009, **3**, 3861–3868.
99 A. Putatunda and D. J. Singh, *Mater. Today Phys.*, 2019, **8**, 49–55.
100 N. T. Hung, A. R. T. Nugraha and R. Saito, *Energies*, 2019, **12**, 4561.
101 B. A. A. Al-Mammory, O. A. Al-Owaedi and E. M. Al-Robayi, *J. Phys.: Conf. Ser.*, 1818, **2021**, 012095.
102 R. M. Al-Utayjawee and O. A. Al-Owaedi, *J. Phys.: Conf. Ser.*, 1818, **2021**, 012208.
103 A. I. M. Obayes, E. M. Al-Robay and O. A. Al-Owaed, *J. Phys.: Conf. Ser.*, 1973, **2021**, 012147.
104 I. A. Shelykh, N. T. Bagraev and L. E. Klyachkin, *Semiconductors*, 2003, **37**, 1390–1399.
105 J. P. Perdew, K. Burke and M. Ernzerhof, *Phys. Rev. Lett.*, 1996, **77**, 3865.
106 J. P. Perdew and Y. Wang, *Phys. Rev. B: Condens. Matter Mater. Phys.*, 1992, **45**, 13244.
107 U. Sivan and Y. Imry, *Phys. Rev. B: Condens. Matter Mater. Phys.*, 1986, **33**, 551.
108 M. D. Hanwell, D. E. Curtis, D. C. Lonie, T. Vandermeersch, E. Zurek and G. R. Hutchison, *J. Cheminform.*, 2012, **4**, 1–17.
109 H. B. J. Schlegel, S. Binkley and J. A. Pople, *J. Chem. Phys.*, 1984, **80**, 1976–1981.
110 D. C. Milan, O. A. Al-Owaedi, M. Oerthel, S. Marqués-González, R. J. Brooke, M. R. Bryce, P. Cea, J. Ferrer, S. J. Higgins, C. J. Lambert, P. J. Low, D. Z. Manrique, S. Martin, R. J. Nichols, W. Schwarzacher and V. M. García-Suárez, *J. Phys. Chem. C*, 2016, **120**, 15666–15674.
111 R. Davidson, O. A. Al-Owaedi, D. C. Milan, Q. Zeng, J. Tory, F. Hartl, S. J. Higgins, R. J. Nichols, C. J. Lambert and P. J. Low, *Inorg. Chem.*, 2016, **55**, 2691–2700.